Hindawi Publishing Corporation
Journal of Ceramics
Volume 2013, Article ID 526434, 8 pages
http://dx.doi.org/10.1155/2013/526434

Research Article

Preparation and Characterization of Nano-Cadmium Ferrite

S. M. Ismail,[1] Sh. Labib,[2] and S. S. Attallah[1]

[1] *Reactor Physics Department, Nuclear Research Center, Egyptian Atomic Energy Authority, P.O. Box 13759, Cairo, Egypt*
[2] *Nuclear Chemistry Department, Hot Laboratories Center, Egyptian Atomic Energy Authority, P.O. Box 13759, Cairo, Egypt*

Correspondence should be addressed to Sh. Labib; shirazmd11@yahoo.com

Received 2 October 2012; Revised 21 December 2012; Accepted 4 January 2013

Academic Editor: Young-Wook Kim

Nano-hematite (α-Fe_2O_3) and nano-cadmium ferrite ($CdFe_2O_4$) are prepared using template-assisted sol-gel method. The prepared samples are analyzed using X-ray diffraction (XRD), Fourier transform infrared spectroscopy (FTIR), scanning electron microscopy (SEM), and Mössbauer spectroscopy techniques for structural and microstructural studies. Nano-α-Fe_2O_3 with particle size ~60 nm is formed at 500°C, while nano-$CdFe_2O_4$ with smaller particle size (~40 nm) is formed at 600°C. It is found that with a simple sol-gel process we can prepare nano-$CdFe_2O_4$ with better conditions than other methods: pure phase at lower sintering temperature and time (economic point) and of course with a smaller particle size. So, based on the obtained experimental results, a proposed theoretical model is made to explain the link between the use of the sol-gel process and the formation of nano-$CdFe_2O_4$ as a pure phase at low temperature. This model is based on a simple magnetostatic interaction between the formed nuclei within the solution leading to the formation of the stable phase at low temperature.

1. Introduction

In recent years, the design and synthesis of nanomagnetic particles has the focus of the intense fundamental and applied research with special emphasis on their enhanced properties that are different from those of their bulk counterparts [1–6]. Nano-cadmium ferrite ($CdFe_2O_4$) is a normal spinel ferrite that can be applied in various fields [7]. Nano-$CdFe_2O_4$ exhibits ferromagnetism, and ~54% of Fe^{3+} ions occupy the A site in contrast to 0% for the bulk materials with normal spinel structures [8]. The enhanced occupancy of Fe^{3+} ions in $CdFe_2O_4$ is explained by a higher octahedral preferential energy of Cd^{2+} [8]. It is found that nano-$CdFe_2O_4$ can be obtained at low temperature by applying solution methods. Desai et al. [8] prepare nano-$CdFe_2O_4$ by sintering at 600°C for 4 h using the precipitation method, where the achieved crystallite size is 43 nm and the hematite (α-Fe_2O_3) as a minor phase is present. Otherwise, Sharma et al. [9] prepare nano-$CdFe_2O_4$, having crystallite sizes (100–200 nm), as a pure phase by sintering at 900°C for 6 h using the urea combustion method. In this paper, nano-$CdFe_2O_4$ is prepared using the sol-gel process that is considered as one of the important methods used in nanoparticles' synthesis. This process is chosen because it gives enhanced homogeneity, better control for size, shape, and degree of agglomeration of the resulting nanocrystals, simple compositional control, and low processing temperature [2, 5, 8, 10–12]. In order to obtain sols and gels with desirable properties, the control of precursor reactivity may be achieved through the addition of chelating agents such as β-diketones, carboxylic acids, or other complex ligands [11, 13]. These characteristics, along with the chemical composition, are found to influence significantly the magnetic properties of nanoferrites [13]. The aim of this paper is to explain theoretically the reason of nano-$CdFe_2O_4$ formation when using the sol-gel process that gives a single phase at both lower sintering temperature and time than that used previously [8, 9]. The prepared nanomagnetic materials are characterized using X-ray diffraction (XRD), Fourier transform infrared spectra (FTIR), scanning electron microscopy (SEM), and Mössbauer effect spectroscopy techniques. Based on the achieved experimental results, a new model is proposed to explain the link between the use of the sol-gel process and the formation of nano-$CdFe_2O_4$ as a pure phase at low temperature.

2. Experimental

2.1. Materials and Method. α-Fe_2O_3 and $CdFe_2O_4$ sols are prepared using $Fe(NO_3)_3{\cdot}9H_2O$ (99% Merck, Germany), $Cd(NO_3)_2{\cdot}4H_2O$ (99% Merck, Germany), isopropyl alcohol (99.8% Scharlau, Spain), acetylacetone (≥99% Merck, Germany), and distilled water. All the used reagents are of AR grade.

(i) α-Fe_2O_3 sol is prepared by a dropwise addition of an alcoholic mixture of isopropyl alcohol (5 mol) and distilled water (2 mol) to the stirred alcoholic solution of $Fe(NO_3)_3{\cdot}9H_2O$ and acetylacetone having molar ratio (isopropyl alcohol/$Fe(NO_3)_3{\cdot}9H_2O$/acetylacetone: 5 : 1 : 2), respectively.

(ii) $CdFe_2O_4$ sol is prepared by a dropwise addition of an alcoholic mixture of isopropyl alcohol (5 mol) and distilled water (2 mol) to the alcoholic mixture of $Fe(NO_3)_3{\cdot}9H_2O$ and $Cd(NO_3)_2{\cdot}4H_2O$ as well as acetylacetone, where $Fe(NO_3)_3{\cdot}9H_2O$ and $Cd(NO_3)_2{\cdot}4H_2O$ are mixed in a stoichiometric ratio (2 : 1), respectively.

The prepared sols are aged for 168 h then dried at 80°C for 48 h and calcined at 400°C for 1 h in the air. The calcined powders are ground for 45 min then pressed uniaxially into tablets at 20 kN. The green compacts are sintered at 500° and 600°C for 3 h in the air. Table 1 shows the abbreviation of the prepared samples.

2.2. Material Characterization. Different compacts are characterized using X-ray diffraction (XRD) (Philips X'pert multipurpose diffractometer), where the used X-ray tube is a copper tube operating at 40 kV and 30 mA and the used wavelength is $K_{\alpha 1}$ with wavelength 1.54056 Å. The scan is performed over the range of 2θ (10–70) degrees. The identification of the present crystalline phases is done using Joint Committee on Powder Diffraction Standards (JCPDS) database card numbers.

Fourier transform infrared spectroscopy (FTIR) analysis (Nicolet iS10 FTIR Spectrometer—Thermo Scientific) is carried out for the prepared powders using KBr disc technique. The scan is performed in the region of 400–4000 cm^{-1}.

Scanning electron microscopy (SEM) for the different samples is employed using JEOL JSM-5600 LV. The scan is performed at high vacuum mode using accelerating voltage 30 kV, working distance 20 mm, and magnification ×3000 and 4000.

Austin Science Mössbauer Spectrometer with constant acceleration laser-interferometer-controlled drive and data acquisition system is used in a standard transmission setup with a Personal Computer Analyzer (PCA II-card with 1024 channels). The radioactive source is ^{57}Co embedded in Rh matrix with initial activity of 50 mCi. Metallic iron spectrum is used for the calibration of both observed velocities and hyperfine magnetic fields. The absorber thickness is approximately 10 mg/cm^2 of natural iron. The Mössbauer effect (ME) spectra are analyzed with a computer program [14], where the analysis of ME spectra for these samples is done using the theories of N magnetic sextets and N quadrupole doublets.

Table 1: Abbreviation of the prepared samples.

Sintering temperature (°C/3 h)	Sample	
	Fe_2O_3	$CdFe_2O_4$
500	F500	CF500
600	F600	CF600

2.3. Theoretical Background. The methods of synthesis based on either chemical or physical concepts allow the structural and microstructural properties of these materials to be highly controlled and to be well reproduced. It is generally agreed that the driving force for a phase transformation is the difference in free energy between the final and the initial states of the system [15]. The driving force for a certain reaction may be written as the derivative

$$-\left(\frac{\partial G}{\partial \xi}\right)_{P,T}, \tag{1}$$

where G is the Gibbs free energy, P and T are pressure and temperature, and ξ is the extent of the reaction.

For the isobarothermal case and fixed composition, the integrated driving force is simply the difference in Gibbs energy between the final and the initial states of the system [15]. On the nanoscale, the phase transformation may involve several processes, for example, migration of coherent, semicoherent, or incoherent phase interface, solute diffusion both inside and ahead of the interface [15]. Each individual process needs some driving force, and the sum of these driving forces can exceed the integrated driving force [15].

For phase transformation with composition change, it is considered integrated force acting on the phase interface [15]. Hillert's analysis yields as the integrated driving force (counted per mole of growing phase)

$$\sum_{J=1}^{n} x_j \Delta\mu_j, \tag{2}$$

where n is the number of components, x_j is the mole fraction of component j in the material that is transferred over the phase interface, and $\Delta\mu_j$ is the difference in chemical potential for j across the phase interface [15].

If there is diffusion in both α and β phases, a different approach is required,

$$x_j = \frac{x_j^{\alpha} J_j^{\beta} - x_j^{\beta} J_j^{\alpha}}{J_j^{\beta} - J_j^{\alpha}}, \tag{3}$$

where x and J, which denote the mole fraction and the diffusion flux, respectively, on each side of the phase interface, can be combined with (2) to give the driving force on the interface in the general case [15]. As concluded, the driving force is expressed not in terms of the total free energy change during crystallization, but rather as the change in

the chemical potential of the crystallization species $\Delta\mu$ [16]. $\Delta\mu$ measures the free energy response to molecules transferring from one phase to the other [16].

It is clear that the determination of the driving force is connected with the evaluation of the thermodynamic properties as a function of composition, temperature, and pressure of a system [15]. Whether considering the nucleation or growth, the reason for the transformation from solution to solid is the same [16]. The free energy of the initial solution phase is greater than the sum of the free energies of the crystalline phase and the final solution phase [16]. As concluded from this brief survey, it is important to correlate the relation between the synthesis mode and the nanophase formation at low temperature based on thermodynamic features. We propose a new model derived from Sacanna et al.'s model [17] to explain the reason of the formation of nano-$CdFe_2O_4$ at low temperature.

3. Results and Discussion

In general, the sol-gel process involves several successive stages: (a) formation of sol which represents a colloidal suspension containing small particles with a diameter less than 1000 nm dispersed in a continuous liquid medium, (b) the gelation of the sol to give a three-dimensional M–O–M/M–OH–M network whose pores are filled with solvent molecules (wet gel), (c) the ageing of the resulting wet gel process known as syneresis, (d) the elimination of the solvent from the gel's pore (drying) [10].

In order to obtain narrow size distribution of nano-Fe_2O_3 and -$CdFe_2O_4$, agglomerations must be prevented during the processing step. So, to produce nanoparticles without agglomeration, a capping agent such as acetylacetone is used to control the particle size and shape, and also ageing time is increased in order to obtain a uniform morphology of the obtained structures [11, 12].

3.1. X-Ray Diffraction (XRD) Analysis. Figure 1 shows the X-ray diffraction pattern of both α-Fe_2O_3 and $CdFe_2O_4$ compacts thermally treated at 500° and 600°C for 3 h. α-Fe_2O_3 is formed at 500°C (JCPDS 79-1741), as shown in Figure 1(a). The obtained hematite phase has a rhombohedral structure with space group $R\overline{3}c$ (167). The broadening of the diffraction peaks suggests that the particle size is very small. The average particle size (D) is 61 nm as given from the Debye-Scherrer equation [18]

$$D = \frac{0.94\lambda}{\beta \cos\theta}, \quad (4)$$

where λ is the wavelength of the X-ray radiation used and β is the full width at half-intensity maximum (FWHM) in radian. The increase in temperature to 600°C yields an increase of the obtained diffraction peaks sharpness due to particle size growth to 69 nm (Figure 1(b)). On the other hand, CF500 compact shows the presence of the cubic $CdFe_2O_4$ phase (JCPDS 79-1155) with minor α-Fe_2O_3 diffraction peaks (Figure 1(c)). The obtained spinel phase has a cubic structure with space group Fd3m (227). The average particle size of $CdFe_2O_4$

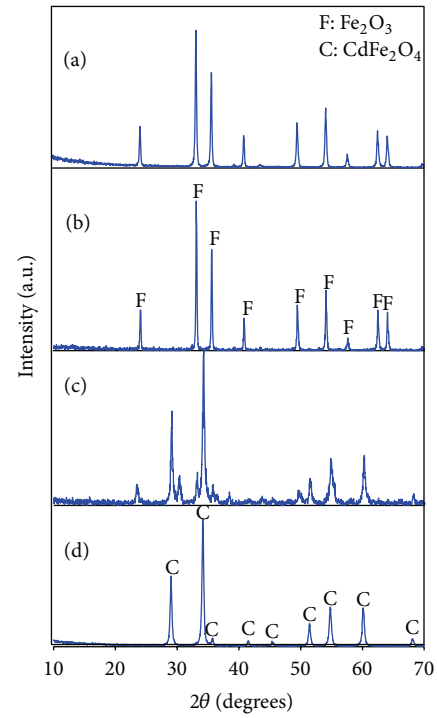

Figure 1: XRD patterns of Fe_2O_3 and $CdFe_2O_4$ compacts thermally treated at 500° and 600°C for 3 h: (a) F500, (b) F600, (c) CF500, and (d) CF600.

phase is 43 nm. CF600 compact shows the disappearance of Fe_2O_3 diffraction lines indicating the complete formation of $CdFe_2O_4$ phase having an average particle size of 48 nm (Figure 1(d)).

In general, the observed decrease in the average particle size of $CdFe_2O_4$ with respect to α-Fe_2O_3 is referred to the strong chemical affinity of Cd^{2+} to the tetrahedral A site and the metastable cation distribution in the nanoscale range of ferrite particles [5]. Based on this feature, one can explain the dependence of particle size on cation stoichiometry [5].

3.2. Fourier Transform Infrared Spectroscopy (FTIR) Analysis. Figure 2 shows the FTIR spectra of both α-Fe_2O_3 and $CdFe_2O_4$ powders thermally treated at 500° and 600°C for 3 h. Figure 2(a) shows the spectrum of F500 powder: a broad band at 3742 cm^{-1} that is assigned to the adsorbed H_2O from the atmosphere or OH group of isopropanol is observed [19, 20].

The very small band at 2300 cm^{-1} is due to adsorbed or atmospheric CO_2 [2, 21]. The characteristic small bands at 1716 and 1338 cm^{-1} are assigned to both asymmetric and symmetric C–O, respectively [2, 19, 21]. The C–O bands region is an indicative of the presence of organic residues due to acetylacetone species [21]. Two small peaks appeared at 533 and 440 cm^{-1} that are characteristic of poorly crystalline α-Fe_2O_3 [19].

The increase in temperature to 600°C shows the disappearance of the band at 3742 cm^{-1} and the increase of the characteristic α-Fe_2O_3 bands intensity (Figure 2(b)).

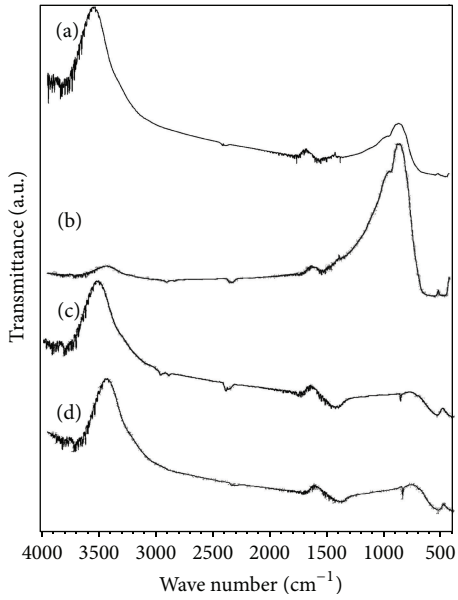

FIGURE 2: FTIR spectra of Fe_2O_3 and $CdFe_2O_4$ powders thermally treated at 500° and 600°C for 3 h: (a) F500, (b) F600, (c) CF500, and (d) CF600.

Figure 2(c) shows the spectrum of CF500 powder, where the bands at 3700, 2359, 1716, and 1450 cm^{-1} are assigned as in the case of the previous samples. Two major sharp bands at 858 and 545 cm^{-1} that are characteristic of spinel ferrite ($CdFe_2O_4$) are observed. The higher frequency band is caused by stretching vibration of the tetrahedral metal-oxygen band (Fe–O), and the lower frequency absorption band is caused by a metal-oxygen stretching vibration in octahedral sites (Cd–O) [21]. The sharpness of these bands is correlated to the high degree of crystallinity of the obtained phase. A very small band at 533 cm^{-1} is observed which is characteristic of poorly crystalline α-Fe_2O_3 as explained previously. This band is indicative of the presence of a minor α-Fe_2O_3 phase as confirmed by X-ray diffraction analysis (Figure 1(c)). A marked decrease in the height of 3700, 2359, 1716, and 1450 bands with increasing the temperature to 600°C is due to the decomposition of all the organic residues (Figure 2(d)) [2, 19]. The characteristic spinel ferrite bands at 858 and 545 cm^{-1} are still present. The Fe_2O_3 band disappears indicating the presence of $CdFe_2O_4$ as a pure phase which is also confirmed by the X-ray diffraction analysis given in Figure 1(d).

3.3. Scanning Electron Microscopy (SEM). SEM measurements are carried out in order to understand the morphology and the shape of the synthesized nanomaterials. SEM micrographs of both nano-α-Fe_2O_3 and -$CdFe_2O_4$ compacts thermally treated at 500° and 600°C for 3 h are shown in Figure 3. F500 is characterized by spherical particles with different sizes that are distributed in a homogeneous manner within fine and small granules (as seen in Figure 3(a)).

F600 is characterized by the presence of both enlarged spherical particles and tiny small spherical particles that are formed from the fine granules (as shown in Figure 3(b)). On the other hand, Figures 3(c) and 3(d) show the SEM of CF500 and CF600 at higher magnification ($x = 4000$) to show the microstructure of nano-$CdFe_2O_4$ particles in detail. The microstructures are characterized by the presence of uniform neck and the bonding of equiaxial grains. An increase in the interparticle spaces of the obtained nanoparticles of CF600 with respect to CF500 is observed (as seen in Figure 3(d)). Two marked features are obtained from SEM illustrations.

(i) The presence of nanoparticles in agglomerated form because in many cases of nanocrystalline ferrites, it is observed that there is a tendency of agglomeration among the nanoparticles [22], consequently, the particle sizes values from SEM do not represent the true particle sizes of the prepared nanoparticles. The aggregated nanoparticles are characterized by uniform shapes which reflect the tailor arrangements of the formed nanocrystallites.

(ii) A decrease in the porous structure of nano-α-Fe_2O_3 with respect to -$CdFe_2O_4$, which is correlated to the particle size increase [23], is the result of individual grains coming closer to each other increasing the effective area of grain to grain contact [23].

3.4. Mössbauer Studies. Figure 4(a) shows the Mössbauer effect (ME) spectrum recorded at room temperature (293 K) for the Fe_2O_3 sample. The figure displays a well-resolved spectrum consisting of one Zeeman sextet due to Fe^{3+}, where Figure 4(b) shows that the spectrum is consisting of one sextet due to the presence of Fe_2O_3 phase with 78% and one doublet of the $CdFe_2O_4$ phase with 22% as clearly shown in this figure. In contrast, the ME spectra at 293 K for $CdFe_2O_4$ ferrite heated at 600°C exhibit quadrupole doublet spectra as illustrated in Figure 5.

3.4.1. Quadrupole Interaction. The presence of chemical disorder in spinel structure produces an electric field gradient (EFG) of varying magnitude, direction, sign, and symmetry and a resulting distribution in the quadrupole splitting (QS). In other words, the EFG at ^{57}Fe nucleus arises from the asymmetrical charge distribution surrounding the ion. However, since an Fe^{3+} ion has a half-filled 3d shell ($3d^5$), the EFG in this case can arise only from an asymmetric charge distribution surrounding the iron ion. Cadmium is known to show strong preference for A sites in spinel ferrites. Consequently, $CdFe_2O_4$ is a normal spinel. This EFG may arise from the departure of the six nearest anion neighbours from their ideal octahedral symmetry and the nonspherical distribution of charges on the next nearest cation and anion neighbours of the B site. In the present work, the QS values at room temperature of the $CdFe_2O_4$ sample are in the range of 0.81 and 0.845 mms^{-1} as shown in Table 2. The values of QS obtained for the $CdFe_2O_4$ at 293 K are in good agreement with those reported earlier in [24].

3.4.2. Isomer Shift. The obtained isomer shift (IS) values for Fe_2O_3 sample and $CdFe_2O_4$ spinel ferrites are given in Table 2. The obtained result of IS is in agreement with other

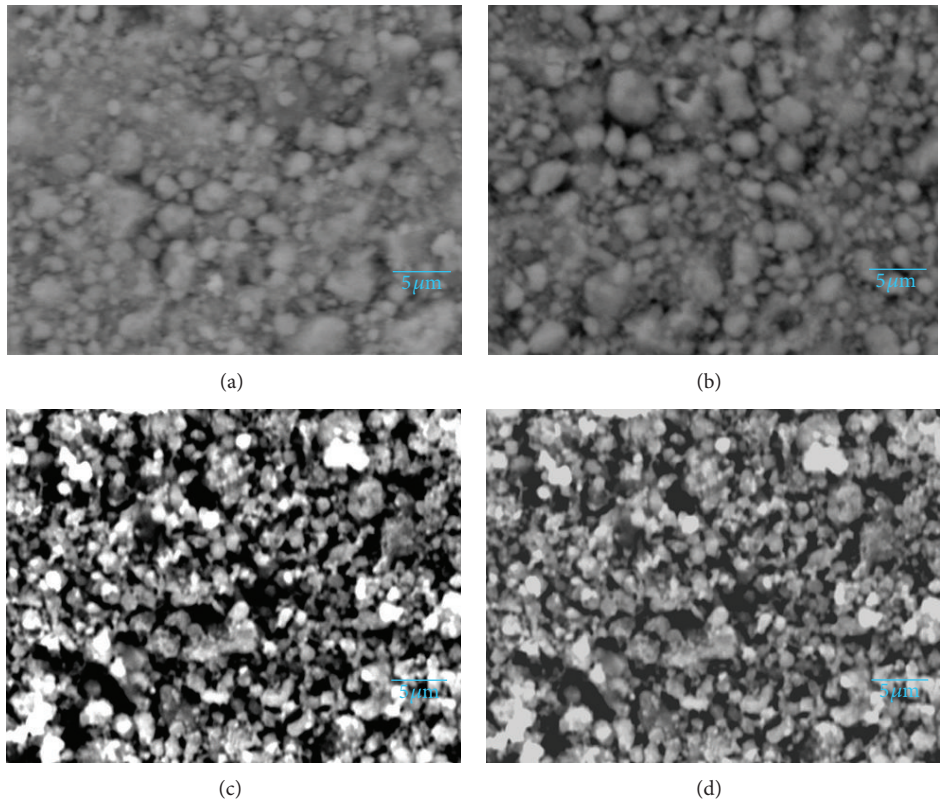

Figure 3: Scanning electron micrograph of Fe_2O_3 and $CdFe_2O_4$ compacts thermally treated at 500° and 600°C for 3 h: (a) F500, (b) F600, (c) CF500, and (d) CF600.

Table 2: Mössbauer parameters for the prepared samples at room temperature.

Sample	H_{hf} (kOe)	QS (mm s^{-1})	IS (mm s^{-1})	Line width Γ (mm s^{-1})	Area ratio (%)
a	515 ± 0.008	−0.215 ± 0.002	0.4964 ± 0.001	0.352 ± 0.004	100
	515.5 ± 0.008	−0.205 ± 0.002	0.514 ± 0.001	0.337 ± 0.004	22
b	—	0.81 ± 0.007	0.5122 ± 0.001	0.378 ± 0.01	78
c	—	0.845 ± 0.002	0.4388 ± 0.001	0.423 ± 0.003	100

previously reported data [24]. This can be interpreted as being due to the large band separation of Fe^{3+}–O^{2-} for the octahedral ions compared with that for the tetrahedral ions. As the orbitals of the Fe^{3+} and O^{2-} ions do not overlap, the covalency effect becomes smaller compared to the isomer shift at the octahedral site in the other spinel ferrite with inverse or partially inverse spinel.

3.4.3. Hyperfine Fields. The hyperfine magnetic field at the iron nucleus is proportional to the spontaneous magnetization of the sublattice to which the particular nucleus belongs. The hyperfine field H_{hf} measured by the ME consists of three contributions: $H_{hf} = H_{core} + H_{dip} + H_{shift}$, where H_{core} results from the polarization of s electrons by the magnetic moments of the d electrons. This field is larger for free ions than for ions in a crystal because of covalency. H_{dip} represents the dipolar fields produced by the surrounding magnetic ions. At room temperature, the hyperfine field H_{hf} value for the Fe_2O_3 sample "treated at 500°C" is 515 ± 0.02 kOe, which is in good agreement with previous work [24, 25]. While, for the $CdFe_2O_4$ sample "treated at 600°C," the intersublattice contributions h_{AB} and h_{BA} are not predominant. So, the paramagnetic doublet is observed as shown in Figure 5.

3.5. Theoretical Proposal. The power of any mode of synthesis is the ability to form nanospinel structure, as a pure phase, at low temperature. A direct correlation exists between the decrease in the Gibbs free energy of the solution and the formation of the nanospinel phase at low temperature as shown in Figure 6.

So, we need to make a model for the synthesis method that explains the decrease of solution's Gibbs free energy and the formation of a nanospinel phase at low temperature.

In the present work, we benefit from the self-assembly model described by Sacanna et al. [17] and modify it to explain our purpose. The assembly model is based on a

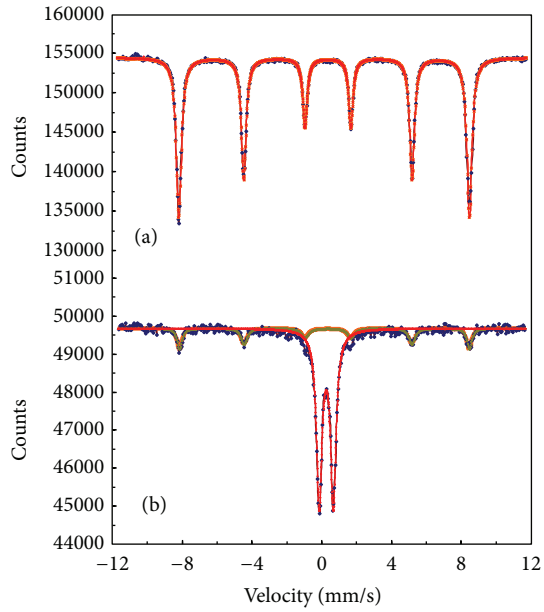

Figure 4: Mössbauer spectra at room temperature for Fe_2O_3 and $CdFe_2O_4$ thermally treated at 500°C for 3 h: (a) F500 and (b) CF500.

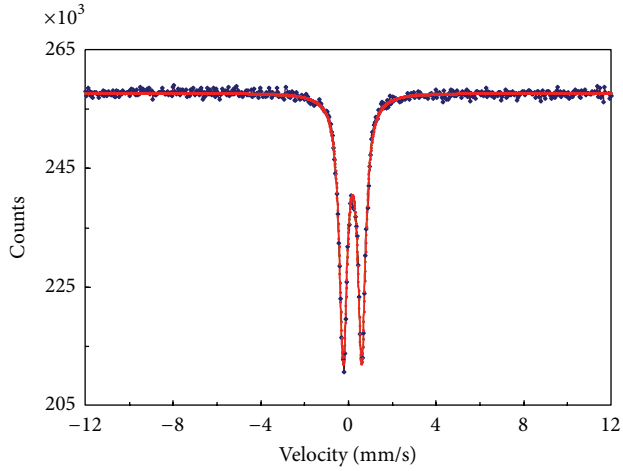

Figure 5: Mössbauer spectrum at room temperature for $CdFe_2O_4$ thermally treated at 600°C for 3 h: CF600.

binding mechanism between colloidal particles using a simple magnetostatic interaction [17]. There is an important reason to investigate this type of interaction, that is, unlike electrostatic and chemical interactions, magnetic forces are not screened in solutions and are independent of the changes in the experimental conditions, thus giving a significant experimental design freedom [17]. The magnetostatic interaction requires particles with localized and well-calibrated magnetic dipole moments [17]. The resulting magnetic forces should be strong enough to bind particles [17]. The model cited by Sacanna et al. describes the degree of dispersion or agglomeration of particles in a colloidal solution by assuming the presence of a magnet (Fe_2O_3) embedded underneath the

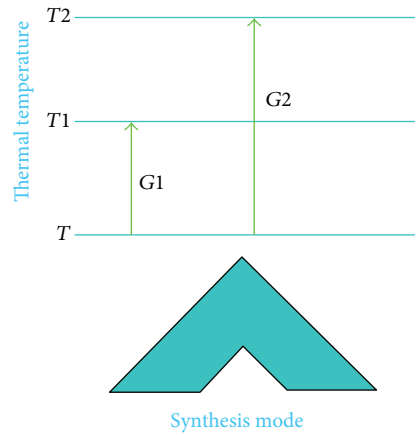

Figure 6: The relation between the decrease of Gibbs free energy and phase formation at low temperature.

particle surface generating localized permanent magnetic dipoles [17].

In order to understand our model, we consider that the used colloidal solution gives the probability of obtaining three phases by sintering at the suitable temperatures: CdO, Fe_2O_3, and $CdFe_2O_4$ phases. In order to obtain nano-$CdFe_2O_4$ phase at low temperature as a pure phase, the Gibbs free energy of $CdFe_2O_4$ formation must be lower than that of CdO and Fe_2O_3 phases.

We consider the presence of both Cd(II) and Fe(III) ions linked together inside the chelating agent as the first nucleus of nanoparticle that breaks up to nanospinel phase by sintering. This nucleus is considered as a magnetic material, due to the presence of Fe(III) ions, that combines with another nucleus via a magnetostatic interaction leading to a more nucleation buildup of the nanospinel phase. By imagining that an oriented nucleus in a certain direction interacts with another one having a different orientation, consequently a building up of nuclei begins to grow sequentially. This imagination is based on considering that each nucleus is a magnet having positive and negative poles and so the unlike poles of different magnets attracts with each other. In this case, a self-magnetic field is generated around the buildup nuclei that are considered as magnets having dipole moments and connected together by a magnetostatic interaction. This self-induced magnetic field is responsible for the formation of the nanospinel phase at low temperature by lowering the Gibbs free energy of the $CdFe_2O_4$ phase formation with respect to that of the CdO and Fe_2O_3 phases. The reason is that many papers are talking about the decrease in the Gibbs free energy of a solution of magnetic particles when an external magnetic field is applied to it [26, 27]. So, the induced magnetic field has a tendency of decreasing the Gibbs free energy of the solution system [26] and so gives the reason of the nanospinel phase formation at low temperature.

The difference between the assembled model and our model is that the assembled model describes the formation of the agglomerated particles in the solution phase instead of the formation of dispersed particles. But here in our model,

the assembled model is used in describing the buildup of nanospinel nuclei; that is, we describe nanophase formation (assembly of nuclei of the nanospinel phase).

4. Conclusion

The aim of this work is to explain theoretically the reason of nano-$CdFe_2O_4$ formation at low temperature when using the sol-gel process for synthesis.

So, nano-Fe_2O_3 and -$CdFe_2O_4$ are prepared using template sol-gel method. The XRD data investigate the formation of nano-Fe_2O_3 and -$CdFe_2O_4$ phases by sintering at 500° and 600°C for 3 h, respectively. Mössbauer studies confirm the results obtained by XRD. SEM illustrations reveal a uniform microstructure of agglomerated nano-Fe_2O_3 and -$CdFe_2O_4$ particles which reflect the tailor arrangements of nanocrystallites. Single-phase nano-$CdFe_2O_4$ (~48 nm) is formed at lower sintering temperature and time than that used in previous methods. A new model is proposed to explain the formation of nano-$CdFe_2O_4$ as a pure phase at low temperature. This model is based on the self-assembled model described by Sacanna et al. By assuming a simple magnetostatic interaction between the formed nuclei that are considered as magnets within the solution, a nanostable phase can be formed at low temperature. The presence of magnetostatic interaction between the nuclei creates a magnetic field, and consequently the Gibbs free energy of the solution is decreased. This explains the formation of $CdFe_2O_4$ as a pure phase at low temperature. Consequently, the assembled model is used in describing the buildup of nanospinel nuclei.

References

[1] Y. L. N. Murthy, I. V. K. Viswanath, T. K. Rao, and R. Singh, "Synthesis and characterization of nickel copper ferrite," *International Journal of ChemTech Research*, vol. 1, no. 4, pp. 1308–1311, 2009.

[2] S. Maensiri, C. Masingboon, B. Boonchom, and S. Seraphin, "A simple route to synthesize nickel ferrite ($NiFe_2O_4$) nanoparticles using egg white," *Scripta Materialia*, vol. 56, no. 9, pp. 797–800, 2007.

[3] S. A. Corr, Y. P. Rakovich, and Y. K. Gun'Ko, "Multifunctional magnetic-fluorescent nanocomposites for biomedical applications," *Nanoscale Research Letters*, vol. 3, no. 3, pp. 87–104, 2008.

[4] P. B. C. Rao and S. P. Setty, "Electrical properties of Ni-Zn nano ferrite particles," *International Journal of Engineering Science and Technology*, vol. 2, no. 8, pp. 3351–3354, 2010.

[5] R. Iyer, R. Desai, and R. V. Upadhyay, "Low temperature synthesis of nanosized $Mn_{1-x}Cd_xFe_2O_4$ ferrites," *Indian Journal of Pure and Applied Physics*, vol. 47, no. 3, pp. 180–185, 2009.

[6] S. P. Gubin, Y. A. Koksharov, G. B. Khomutov, and G. Y. Yurkov, "Magnetic nanoparticles: preparation, structure and properties," *Russian Chemical Reviews*, vol. 74, no. 6, pp. 489–520, 2005.

[7] P. K. Nayak, "Synthesis and characterization of cadmium ferrite," *Materials Chemistry and Physics*, vol. 112, no. 1, pp. 24–26, 2008.

[8] R. Desai, R. V. Mehta, R. V. Upadhyay, A. Gupta, A. Praneet, and K. V. Rao, "Bulk magnetic properties of $CdFe_2O_4$ in nano-regime," *Bulletin of Materials Science*, vol. 30, no. 3, pp. 197–203, 2007.

[9] Y. Sharma, N. Sharma, G. V. S. Rao, and B. V. R. Chowdari, "Li-storage and cycling properties of spinel, $CdFe_2O_4$, as an anode for lithium ion batteries," *Bulletin of Materials Science*, vol. 32, no. 3, pp. 295–304, 2009.

[10] D. Caruntu, *Nanocrystalline transition metal ferrites: synthesis, characterization and functionalization [Ph.D. thesis]*, University of New Orleans, 2006.

[11] M. Cernea, "Sol-gel synthesis and characterization of $BaTiO_3$ powder," *Journal of Optoelectronics and Advanced Materials*, vol. 7, no. 6, pp. 3015–3022, 2005.

[12] M. A. Willard, L. K. Kurihara, E. E. Carpenter, S. Calvin, and V. G. Harris, "Chemically prepared magnetic nanoparticles," *International Materials Reviews*, vol. 49, no. 3-4, pp. 125–170, 2004.

[13] C. Sanchez, J. Livage, M. Henry, and F. Babonneau, "Chemical modification of alkoxide precursors," *Journal of Non-Crystalline Solids*, vol. 100, no. 1–3, pp. 65–76, 1988.

[14] S. S. Ata-Allah, M. K. Fayek, H. S. Refai, and M. F. Mostafa, "Mossbauer effect study of copper containing nickel-aluminate ferrite," *Journal of Solid State Chemistry*, vol. 149, no. 2, pp. 434–442, 2000.

[15] K. Thornton, J. Ågren, and P. W. Voorhees, "Modelling the evolution of phase boundaries in solids at the meso- and nano-scales," *Acta Materialia*, vol. 51, no. 19, pp. 5675–5710, 2003.

[16] P. Mathur, A. Thakur, and M. Singh, "Synthesis and characterization of $Mn_{0.4}Zn_{0.6}Al_{0.1}Fe_{1.9}O_4$ nano-ferrite for high frequency applications," *Indian Journal of Engineering and Materials Sciences*, vol. 15, no. 1, pp. 55–60, 2008.

[17] S. Sacanna, L. Rossi, and D. J. Pine, "Magnetic click colloidal assembly," *Journal of the American Chemical Society*, vol. 134, no. 14, pp. 6112–6115, 2012.

[18] B. D. Cullity, *Elements of X-Ray Diffraction*, Addison-Wesley, Reading, Mass, USA, 2nd edition, 1978.

[19] M. A. Gabal, A. A. El-Bellihi, and S. S. Ata-Allah, "Effect of calcination temperature on Co(II) oxalate dihydrate-iron(II) oxalate dihydrate mixture: DTA-TG, XRD, Mössbauer, FT-IR and SEM studies (part II)," *Materials Chemistry and Physics*, vol. 81, no. 1, pp. 84–92, 2003.

[20] S. W. Boland, S. C. Pillai, W.-D. Yang, and S. M. Haile, "Preparation of (Pb, Ba) TiO_3 powders and highly oriented thin films by a sol-gel process," *Journal of Materials Research*, vol. 19, no. 5, pp. 1492–1498, 2004.

[21] R. W. Schwartz, J. A. Voigt, B. A. Tuttle, D. A. Payne, T. L. Reichert, and R. S. DaSalla, "Comments on the effects of solution precursor characteristics and thermal processing conditions on the crystallization behavior of sol-gel derived lead zirconate titanate thin films," *Journal of Materials Research*, vol. 12, no. 2, pp. 444–456, 1997.

[22] S. A. Khorrami, G. Mahmoudzadeh, S. S. Madani, and F. Gharib, "Effect of calcination temperature on the particle sizes of zinc ferrite prepared by a combination of sol-gel auto combustion and ultrasonic irradiation techniques," *Journal of Ceramic Processing Research*, vol. 12, no. 5, pp. 504–508, 2011.

[23] M. A. Ahmed, N. Okasha, and S. I. El-Dek, "Preparation and characterization of nanometric Mn ferrite via different methods," *Nanotechnology*, vol. 19, no. 6, Article ID 065603, 6 pages, 2008.

[24] J. Plocek, A. Hutlová, D. Nižňanský, J. Buršík, J.-L. Rehspringer, and Z. Mička, "Preparation of $ZnFe_2O_4/SiO_2$ and $CdFe_2O_4/$

SiO_2 nanocomposites by sol-gel method," *Journal of Non-Crystalline Solids*, vol. 315, no. 1-2, pp. 70–76, 2003.

[25] A. Lančok, P. Bezdička, M. Klementová, K. Závěta, and C. Savii, "Fe_2O_3/SiO_2 hybrid nanocomposites studied mainly by Mössbauer spectroscopy," *Acta Physica Polonica A*, vol. 113, no. 1, pp. 577–581, 2008.

[26] X. J. Liu, Y. M. Fang, C. P. Wang, Y. Q. Ma, and D. L. Peng, "Effect of external magnetic field on thermodynamic properties and phase transitions in Fe-based alloys," *Journal of Alloys and Compounds*, vol. 459, no. 1-2, pp. 169–173, 2008.

[27] Y. Zhang, C. He, X. Zhao, L. Zuo, C. Esling, and J. He, "New microstructural features occurring during transformation from austenite to ferrite under the kinetic influence of magnetic field in a medium carbon steel," *Journal of Magnetism and Magnetic Materials*, vol. 284, no. 1–3, pp. 287–293, 2004.